AIP | Review of Scientific Instruments

Optimized mirror shape tuning using beam weightings based on distance, angle of incidence, reflectivity, and power

Kenneth A. Goldberg and Valeriy V. Yashchuk

Citation: Review of Scientific Instruments **87**, 051805 (2016); doi: 10.1063/1.4950747
View online: http://dx.doi.org/10.1063/1.4950747
View Table of Contents: http://scitation.aip.org/content/aip/journal/rsi/87/5?ver=pdfcov
Published by the AIP Publishing

Optimized mirror shape tuning using beam weightings based on distance, angle of incidence, reflectivity, and power

Kenneth A. Goldberg[1,a)] and Valeriy V. Yashchuk[2]
[1]*Center for X-Ray Optics, Lawrence Berkeley National Laboratory, Berkeley, California 94720, USA*
[2]*Advanced Light Source, Lawrence Berkeley National Laboratory, Berkeley, California 94720, USA*

(Received 5 January 2016; accepted 2 April 2016; published online 24 May 2016)

For glancing-incidence optical systems, such as short-wavelength optics used for nano-focusing, incorporating physical factors in the calculations used for shape optimization can improve performance. Wavefront metrology, including the measurement of a mirror's shape or slope, is routinely used as input for mirror figure optimization on mirrors that can be bent, actuated, positioned, or aligned. Modeling shows that when the incident power distribution, distance from focus, angle of incidence, and the spatially varying reflectivity are included in the optimization, higher Strehl ratios can be achieved. Following the works of Maréchal and Mahajan, optimization of the Strehl ratio (for peak intensity with a coherently illuminated system) occurs when the expectation value of the phase error's variance is minimized. We describe an optimization procedure based on regression analysis that incorporates these physical parameters. This approach is suitable for coherently illuminated systems of nearly diffraction-limited quality. Mathematically, this work is an enhancement of the methods commonly applied for *ex situ* alignment based on uniform weighting of all points on the surface (or a sub-region of the surface). It follows a similar approach to the optimization of apodized and non-uniformly illuminated optical systems. Significantly, it reaches a different conclusion than a more recent approach based on minimization of focal plane ray errors. *Published by AIP Publishing.* [http://dx.doi.org/10.1063/1.4950747]

I. INTRODUCTION

Numerous scientific investigations in materials science, chemistry, and biology rely on highly concentrated beams of X-ray and other short-wavelength light as nanometer-scale probes of the properties of matter. To create advanced experimental systems and realize the potential of existing and emerging high-brightness light sources, researchers have been working continuously on the refinement of metrology and mirror shaping tools capable of meeting sub-100-nrad mirror slope error specifications and beyond. The control and use of concentrated X-ray light has been the goal of *in situ* and *ex situ*, visible-light and at-wavelength metrology efforts for several decades. Metrology is gaining increasing importance as new and upgraded synchrotrons and free-electron lasers offer beams of higher brightness and higher coherence, including emerging diffraction limited sources.

For short-wavelength applications, glancing-incidence mirrors are among the most common beam focusing elements for several important reasons. Below the critical angle, reflectivity from smooth surfaces is high for short-wavelength light. At low angles, a high-power beam of light can be distributed across a large surface area, facilitating cooling and temperature control and reducing the incident power density. Finally, at glancing angles of incidence, tolerance to mirror surface shape errors and imperfections improves, allowing the mirror height error specifications to be greatly relaxed in the longitudinal direction and even more so in the lateral direction.

Glancing incidence mirrors used for nano-focusing have several unusual optical properties that affect optimization efforts. (1) The near and far edges of the mirror can have significantly different distances from focus. (2) Unlike on-axis optical systems, the angle of incidence changes asymmetrically across the pupil. (3) Efforts to utilize all of the available light and to achieve the highest quality surfaces lead to designs where the beam power is concentrated near the middle of the pupil and may fall-off significantly toward the edges. (4) Reflectivity may vary spatially due to angle- and wavelength-dependent coating properties and due to contamination or damage. In this article, we show how these and other physical factors can be incorporated in general optimization procedures to improve focusing.

Previous work in this area[1,2] included the linear distance from focus (i.e., the *ray* error) in the weighting applied to mirror surface shape optimization.[3,4] The geometric argument in favor of this weighting was based on the observation that slope errors on the mirror surface, farther from focus, would deflect rays by a larger lateral distance; while slope errors closer to focus deflect rays to a smaller distance. Further study, including a wave optical approach to beam propagation, now shows that the situation is not so simple. For coherently illuminated optical elements performing at nearly diffraction-limited quality, the diffraction integral dictates the focusing properties and must be considered.

Hypothetically, if a mirror were able to conform to the ideal shape and position, then no further optimization would be possible, and the given optimization would be ideal for *any* incident power distribution and configuration. In practice, the presence of surface shape errors that cannot be fully

a)Electronic mail: kagoldberg@lbl.gov

compensated by mirror alignment and actuation gives rise to the problem of shape optimization.

When certain degrees of freedom are available for optimization, the best focusing performance will be achieved when the mirror is tuned into a shape that maximizes the intensity on axis (i.e., Strehl ratio[5,6]). For small errors, Maréchal,[7] Mahajan,[8] and others have shown that this occurs when the expectation value of the phase-error variance is minimized. Numerous researchers have approached the related questions of aberration balancing in the presence of apodization,[9,10] non-uniform beam intensity,[9,11,12] and various pupil shapes.[6,8,9,13]

It stands to reason that where no light falls, the shape of a beam-focusing mirror is irrelevant, and the weighting can be set to zero in the error minimization calculation. In a similar way, the physical effects that mediate the spatially varying contributions to focusing, from points across the mirror surface, can be included in the shape optimization procedure. We show that such an optimization, using spatially varying weightings, can easily be incorporated into glancing-incidence mirror tuning procedures based on least-squares minimization or (equivalently) linear regression, which are deterministic, non-iterative solutions.

We note that other error minimization approaches, outside the scope of this discussion, have been applied to systems of greater complexity, where the physical limitations of bending and actuation are not ignored.[14] The optimization of mirror shapes based directly on slope measurements is also possible; but it is the wavefront phase variance, calculated from the mirror height error and other physical factors, that is directly connected to the intensity at focus through the Strehl ratio.

II. CALCULATING THE INTENSITY IN THE FOCAL PLANE

Considering coherent, quasi-monochromatic mirror illumination from a point-like light source, the distribution of light intensity in the focal plane (actually, in any plane) can be calculated by summing the coherent electric-field contributions from all waves reaching the points therein and taking the square modulus of the result. We can greatly simplify the problem by treating any aberrated and/or misaligned mirror as a perturbation of the ideal, focused state. Our physical optics approach uses wave propagation from the coherent, point-like source to the mirror, and then to the focal plane. Small errors in the surface shape (i.e., height) are included by the phase error (optical path length error) they induce. Special attention is paid to the varying amplitude of the field at all points in the calculation. The focal plane field calculation relies on a finely sampled array of points to model the coherent wavefront's properties.

For example, consider a single elliptical mirror from a Kirkpatrick-Baez (KB) pair[15]—a common configuration used to focus light in two dimensions on X-ray beamlines. In one dimension, the object and image points occupy the two conjugate foci of the parent ellipse, and the position of the mirror determines the magnification of the system. In the ideal design, a diverging cylindrical wave emanating from the object point reaches all points on the mirror surface. The wave is reflected by the curved mirror with precisely the correct phase relationship (i.e., the correct optical path lengths) to produce a cylindrically *converging* wave front centered on the image point. From this description, we know the ideal phase (or optical path length) for every point on the mirror; we can therefore restrict our calculations to the propagation of light from the mirror to the focal plane. In other words, knowing that the ideal configuration produces a cylindrical wavefront makes a detailed consideration of the (ideal) incident wave unnecessary. Small surface shape errors or misalignments change the phase in a deterministic way that we can include in our model.

A. Surface height errors

In the propagation of coherent beams, the wavefront phase error is related to the optical path length, or more importantly, the *optical path difference* seen by rays interacting with the all of the points across the beam. At each point where the light reaches the mirror surface, the mirror's local height error determines the path length difference (and therefore the phase error) in a straightforward way. The influence of various height error magnitudes and spatial frequencies is all included in the wavefront propagation model provided that the spatial sampling in the calculation is dense enough to preserve the wave nature. This approach links geometrical optics with wave optics and allows us to confine our discussion to surface height errors rather than slope errors.

Figure 1 shows how a reflected ray's path is changed in the presence of a surface error with height h. When h is small, the path length change, Δs, may be calculated as,

$$\begin{aligned}\Delta s &= b - a \\ &= \frac{h}{\sin\theta}(1-\cos 2\theta) = 2h\sin\theta \approx 2\,\theta h. \end{aligned} \tag{1}$$

With glancing-incidence, θ values are commonly smaller than 100 mrad—often much smaller. The path length difference can therefore be an order of magnitude smaller than the height error, h. The corresponding wavelength-dependent phase error ϕ is $4\pi\theta h/\lambda$, or $2k\theta h$, with wavenumber, k.

B. Intensity at focus

Under coherent illumination, the light-intensity at points in the focal plane can be calculated by integrating contributions from each point on the mirror surface, weighted by physical

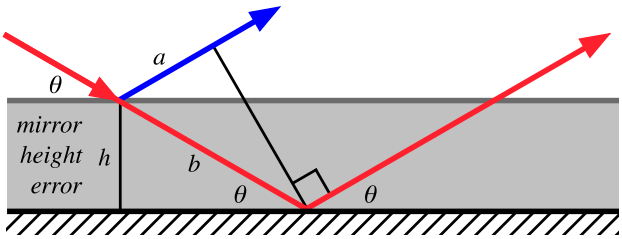

FIG. 1. A height error on the mirror surface changes the path of a reflected ray from the ideal (red) path to a new path shown in blue.

factors related to the amplitude of the field at each point. Following the Huygens-Fresnel principle, we calculate the intensity at positions in the plane containing the focus, and normal to the central ray—or equivalently, in any convenient sample plane where the intensity distribution is sought. (A related approach has recently been pursued by Raimondi and Spiga, under stronger approximations, and for rotationally symmetric systems.[16,17]) The geometry is shown in Fig. 2. Points in this plane are labeled with lateral position, p. Points along the mirror surface are referenced by coordinate, x. In practice, each position, x, has a two-dimensional location along the mirror's surface, including all aberrations and misalignments. Here, we constrain our discussion to one dimension for simplicity.

The diffraction integral[18,19] is used to calculate the coherent superposition of all contributions to the field at a point, p_0. Owing to the small numerical aperture values typically used in glancing-incidence systems, polarization plays little to no role, and scalar wave propagation is suitable for this calculation. All of the physical properties that contribute to the wave amplitude of the light reflected from each point on the mirror surface are gathered into $A(x)$,

$$I(p_0) = \left| \frac{1}{i\lambda} \int_L A(x) \frac{\exp\{ik[s(x,p_0) - s_0(x,0)]\}}{s(x,p_0)} \cos(x,p_0) dx \right|^2. \tag{2}$$

Here, $s(x, p_0)$ is the distance between points on the true mirror surface and a given point in the focal plane while $s_0(x, 0)$ is the ideal distance from points on the mirror to the focal position. The cos Θ term is the *obliquity factor* calculated for the angle between the ideal ray propagation direction (toward focus) and the aberrated ray angle. In all cases relevant to this discussion, we are considering points in the immediate vicinity of the ideal focus, so Θ is nearly zero, and this factor can be neglected,

$$I_0 \sim \left| \int_L A(x) \frac{\exp[i\phi(x)]}{s(x)} \, dx \right|^2. \tag{3}$$

In this way, $A(x)$ and $s(x)$ play a combined role in weighting the contributions from points on the mirror surface. Note that it is possible for surface contamination to contribute both amplitude and phase errors. Those effects, if known, can also be captured in a complex-valued $A(x)$ without loss of generality.

Finally, to simplify the representation of the weighting, we can combine $A(x)$ and $s(x)$ into a single weighting, $A_C(x) = A(x)/s(x)$, giving us

$$I_0 \sim \left| \int_L A_C(x) \exp[i\phi(x)] \, dx \right|^2. \tag{4}$$

We note that a somewhat more complex description of the intensity arises in the case of incoherent or partially coherent illumination, which occurs with extended source sizes. A conventional approach is to incoherently sum the contributions of coherent calculations made for independent points within the source distribution. In such cases, the Strehl ratio optimization is still relevant but the intensity calculation is somewhat different than what we describe.

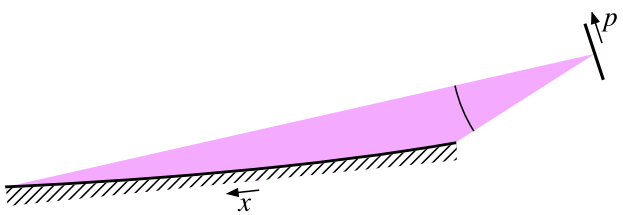

FIG. 2. The geometry of light propagation from the mirror surface to the focal plane.

III. PHYSICAL WEIGHTING

We believe that there are several most-significant factors affecting nano-focusing that must be taken into account in the calculation of the focal plane intensity pattern. These are enumerated below and illustrated in Fig. 3. Other factors may arise in special cases and can be included in a manner similar to this description.

Here we take as an example a single, elliptically shaped bendable mirror used by the authors in metrology experiments at Advanced Light Source beamline 5.3.1.[1,2] The specifications are as follows: r = 1600 mm (object distance), r' = 120 mm (image distance), L = 120 mm (mirror length), θ_g = 8 mrad (central glancing angle), λ = 1 nm (wavelength), $NA_{max} \approx 0.004$ (numerical aperture).

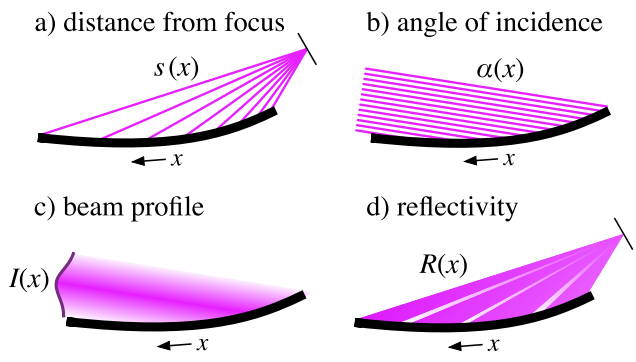

FIG. 3. Weighting in the focal plane intensity calculation is primarily affected by four physical properties. The x coordinate is along the mirror surface and follows any convenient direction or reference.

The factors can be generalized as follows.

A. Distance

The distance to focus, $s(x)$, can vary by a factor of 3 or greater. In our example, it changes from 60 to 180 mm, affecting the weighting by a factor of $^2/_3$ to 2 with respect to the weighting at the geometric center of the mirror.

B. Angle

The angle of incidence, $\theta(x)$, changes from 6.7 to 11.1 mrad, varying by factors of 0.83–1.39 with respect to the angle at the geometric center. Even with a uniform beam-intensity cross section, the angle of incidence affects the power density by spreading the beam over a larger or smaller mirror area.

C. Intensity

The beam intensity profile, $I(x)$, can take a variety of forms. It can be "zero" at the edges due to (1) the finite extent of the mirror, (2) beam-limiting apertures, or (3) a gradual roll-off of the beam's intensity. In cases where the collection of every available photon is important to the signal-to-noise ratio of the experiment, it is common for the mirror aperture to exceed the beam size. It is also common to restrict the aperture with slits to limit light to the higher-quality, central regions of the mirror surface.

D. Reflectivity

The reflectivity, $R(x)$, can vary spatially due to wavelength and angle-dependent coating properties and by the presence of imperfections or contamination.

E. Complex contributions

The methodology presented here generally considers weighting functions with real-valued contributions, such as reflectance, intensity, and distance. Other factors may arise that contribute complex-valued (i.e., phase) errors to the mirror focusing in addition to the weighting. Such considerations are challenging to assess with *ex situ* metrology, and in those cases will fall outside of the scope of this discussion.

F. *Ex situ* vs. at-wavelength *in situ* metrology

Consideration of these physical factors would apply to either *ex situ* metrology performed with visible-light, for example,[3] or *in situ* metrology performed at the operational wavelength of the mirrors.[1,2] *In situ* wavefront measurements can base the weighting on the beam intensity profile measured in a plane that is ahead of or beyond focus. Measuring intensity in this way inherently combines the incident beam profile, the angle of incidence, and spatially varying reflectivity considerations. For *in situ* measurements, the varying distance from focus can be included in the optimization calculation by mapping the measured weighting profile back onto to the mirror's surface.

IV. EXAMPLES SHOWING THE ROLE OF DISTANCE WEIGHTING

Two examples presented here reveal the importance of distance weighting in mirror shape optimization. They show that similar, localized shape errors on different parts of the mirror surface yield significantly different focusing outcomes.

Calculations in these examples are performed with the methodology of Section II, Eq. (4), using phase errors computed from the height errors and the angle of incidence, point by point, as in Section II A. Of the physical weightings described in Section III, the variable distance from focus and the power density's dependence on the angle of incidence are applied. We assume uniform illumination intensity cross section and uniform reflectivity at all points along the mirror. All calculations are made with 1-nm wavelength (1240 eV).

We begin with the ideal mirror geometry for the single elliptical mirror described in Section III. We explore two types of localized mirror surface height errors occurring at various positions along the mirror surface: wedge-shaped slope errors and Gaussian-shaped errors. The height errors introduced to the mirror surface behave as wavefront phase errors in focusing, following Eq. (1).

A. Localized tilt errors

Consider a surface shape error that has a wedge-like profile, with a constant (relatively large) slope error of 12.5-μrad magnitude, extending over one-fifth of the mirror's length. This situation turns the ideal mirror into two mirrors with a slight tilt between them, and one having four times the area of the other. In five separate calculations, labeled "a" through "e," the finite wedge is positioned at different locations on the mirror, as shown in Fig. 4(a). To isolate position-dependent effects, we assume uniform illumination and reflectivity across the mirror surface. The calculated intensity patterns in the focal plane are shown in Figs. 4(b) and 4(c).

In all cases, 80% of the mirror is un-aberrated and produces a normal focal spot. The various tilted portions produce a displaced, secondary focus with lower intensity. The differences among these cases can be explained by Eq. (3). From the perspective of ray optics, the tilted portion deflects light by the same angle error in each case, and the varying distance to focus controls the magnitude of the lateral displacement. At the same time, the reciprocal distance in the integral leads to a decrease in the relative influence of the upstream aberrations.

While the slope magnitude considered here is large on the scale of nearly diffraction-limited, state-of-the-art mirrors, it illustrates the point that the same error shape, at different positions on the mirror surface, produces different results. Additional calculations show that smaller slope errors, down to about 2 μrad, produce similar changes in the Strehl ratios but displace the secondary peaks by smaller distances. The reason is that once the slope of a given tilt error is large enough to send light outside of the central peak, the power reduction observed at focus is approximately unchanged.

The calculated Strehl ratios show the varying influence of the location of the isolated aberrations. With 20% of the

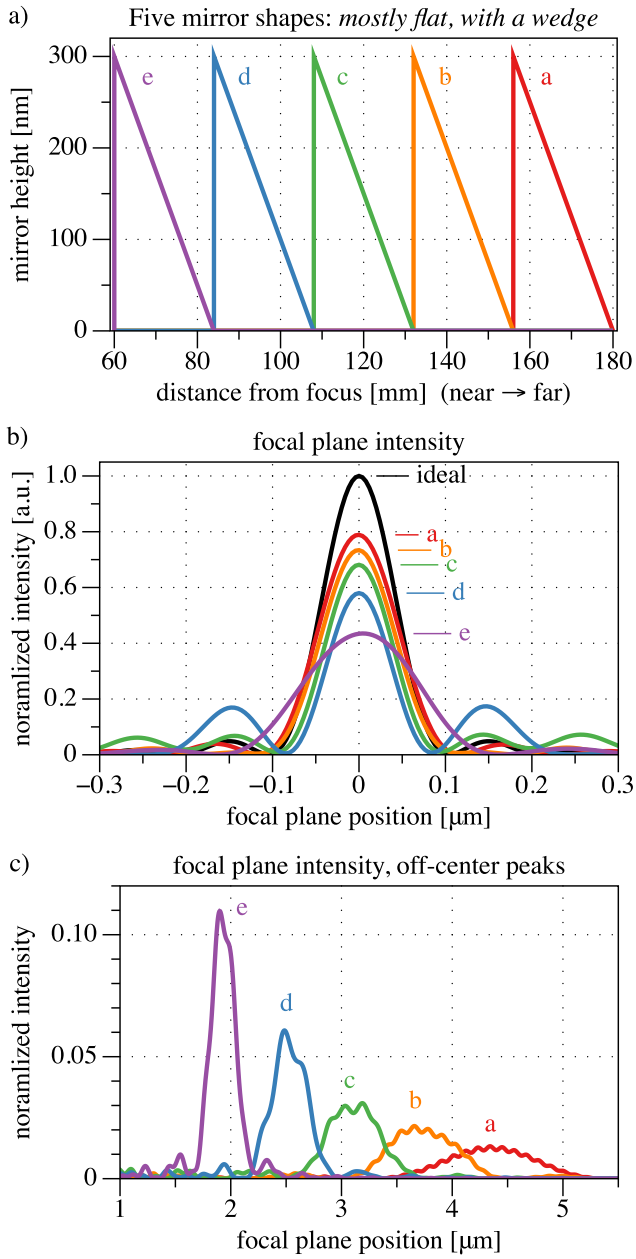

FIG. 4. (a) Example mirror surface height error with a localized slope error along 1/5th of the mirror surface, but shifted to different locations in the five examples, a through e. (b) Calculated focal plane intensity near the center, normalized to the maximum intensity of the un-aberrated focus. (c) Off-axis side-lobe peaks coming from the tilted portion of the mirror. The position and peak intensity of the side-lobe varies with the position of the tilt aberration.

mirror area directing light away from focus, 0.800 should be the highest ratio we could expect. The un-aberrated 80% of the mirror surface contributes to focusing, and the differences in distance from focus and angle of incidence affect the Strehl ratio in this example. In cases "a" through "e," the Strehl ratios are {0.789, 0.734, 0.681, 0.580, 0.435}, respectively. These calculations show that due to the distance and angle dependence, the upstream aberrations (farthest from focus) subtract less power from the central peak than the downstream aberrations. Conservation of energy dictates that the power lost in the central peak is equal to the power directed into the rest of the focal plane, primarily into the second peak.

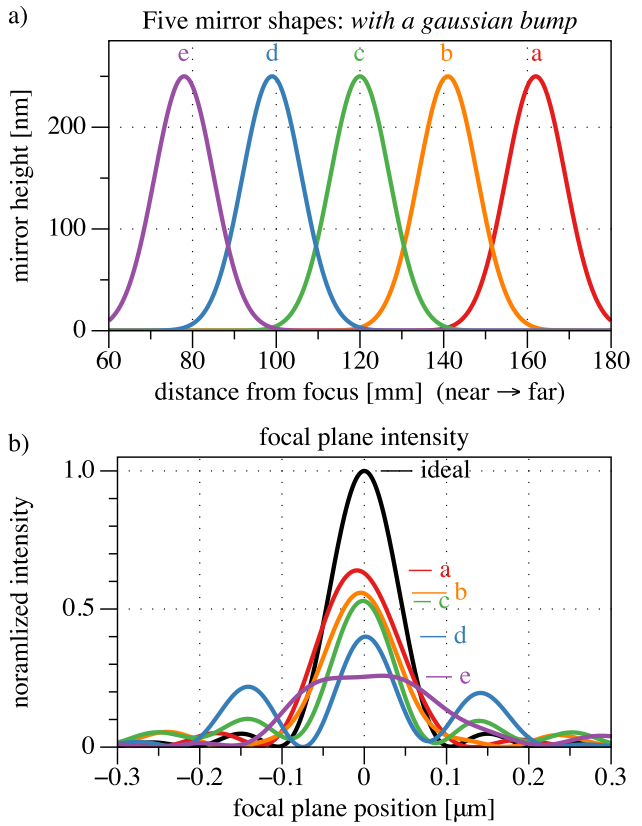

FIG. 5. (a) Example mirror surface height error with a Gaussian profile in five different positions on the mirror surface, a through e. (b) Calculated focal plane intensities showing differences that are dependent on the position of the Gaussian error.

B. Localized Gaussian errors

A similar set of experiments places five Gaussian-shaped mirror height aberrations onto different positions on the mirror (Fig. 5(a)) and calculates the intensity near focus (Fig. 5(b)). The errors have peak magnitudes of 250 nm with peak slope of 21.4 μrad. Here, the Strehl ratios for cases "a" through "e" are {0.640, 0.559, 0.529, 0.400, 0.258}, respectively. Again, the upstream aberrations have a smaller influence on the intensity at focus than the similar, downstream aberrations due to the distance and angle of incidence.

V. MAXIMIZING THE STREHL RATIO

The Strehl ratio measures the performance of an imperfect, coherently illuminated imaging system by comparing the central irradiance to that of an ideal, un-aberrated system of the same design. Use of the Strehl ratio as a metric for focusing and optimization is most effective when the system is capable of achieving close to diffraction-limited quality, and thus forms a single, central intensity peak. Indeed for optimized systems where the light at focus forms multiple peaks or an extended peak shape, the Strehl Ratio loses meaning. For this reason, we confine this discussion to high-quality systems. In more complex cases, including those with partially coherent illumination, wavefront propagation calculations, such as those described by Chubar *et al.*[20,21] and by Yashchuk *et al.*,[22] may be necessary.

Several authors, in particular Szapiel,[23,24] Mahajan,[8,11,25] and Herloski,[12] discussed the classical Strehl ratio–Maréchal intensity formula for determination of imaging properties. Mahajan[8] writes this ratio, S, as

$$S = I(0)_{\phi}/I(0)_{\phi=0} = |\langle \exp(i\phi)\rangle|^2. \quad (5)$$

Here, in Mahajan's notation, $I(0)$ is the peak intensity at focus, and ϕ represents a non-ideal, aberrated wavefront ($\phi = 0$ is the ideal case). The angle brackets indicate a spatial average over the amplitude-weighted pupil. The spatial average of a parameter $f(x)$ is given by

$$\langle f\rangle = \int A(x)\, f(x)\, dx \Big/ \int A(x)\, dx, \quad (6)$$

with weighting distribution function $A(x)$ representing all physical components of the amplitude weighting and with the integral performed over the pupil.

While Mahajan's cited work gave examples of annular pupil shapes, Herloski and others addressed non-uniform (e.g., Gaussian) illumination profiles. The Strehl description holds in all cases and leads to a common result. Following Mahajan, expansion of the exponential for small aberrations gives the Maréchal formula

$$S \gtrsim \left(1 - \frac{1}{2}\sigma_{\phi}^2\right)^2. \quad (7)$$

Where $\sigma_{\phi}{}^2$ is the variance of the wavefront phase aberration. Further expansion, neglecting 4th order terms, leads to a familiar result used by numerous authors in the discussion of orthogonal wavefront aberrations.

$$S \gtrsim 1 - \sigma_{\phi}^2. \quad (8)$$

Maximizing the Strehl ratio in these cases therefore comes down to minimizing the variance of the aberrations. The variance of $\phi(x)$ may be expressed as

$$\sigma_{\phi}^2 = \langle \phi^2\rangle - \langle \phi\rangle^2. \quad (9)$$

The phase can be defined with respect to a constant offset so that $\langle\phi\rangle = 0$, simplifying the optimization to the minimization of $\langle\phi^2\rangle$.

In our context, the minimization follows from Eq. (6), using the single, combined weighting function, $A_C(x)$, from Eq. (4). In general, mirror alignment (rigid-body motions) and shape actuation or bending allow $\phi(x)$ to be adjusted continuously (over a small range) while $A_C(x)$ either remains fixed or varies slowly. This observation allows the minimization of $\langle\phi^2\rangle$ to occur independent of the denominator of Eq. (6).

The minimum of $\langle\phi^2\rangle$ will coincide with the minimum of $\int A_C(x)[\phi(x)]^2 dx$. Since $\phi = 2k\theta h$, this will occur at the minimum of $\int A_C(x)[\theta(x)h(x)]^2 dx$ to which it is proportional. (Again, θ is the glancing angle of incidence, and h is the height error, and ϕ is the resultant wavefront phase error.) If the $\theta(x)$ term is nearly constant, it can be ignored in the minimization. Otherwise, θ^2 can be grouped with $A_C(x)$ as part of the complete weighting. Thus, maximizing the Strehl ratio is equivalent to minimizing $\int A_C(x)[h(x)]^2 dx$.

A. Optimization with characteristic functions

There are a wide variety of actuators, bending mechanisms, and mirror-holding stages that can be applied to adjust the shape and position of X-ray mirrors *in situ*. To demonstrate the optimization described above, we introduce it to the *method of characteristic* functions.[2–4,26] When the mirror is close to its optimal configuration, small, independent actuations produce measurable changes in the mirror height profile, separately for every available degree of freedom. These changes are called the characteristic functions of each actuator, and there are N functions for N actuators.

This approach is robust when actuation is linear, repeatable, and the degrees of freedom are non-degenerate. The characteristic functions can be measured and applied in a strictly empirically way, making it a practical approach for optimization in a wide variety of optical systems. Feedback can come from *ex situ* or *in situ* surface height (or slope) measurements, and the method produces internally consistent results.

Mathematically equivalent optimizations can be performed with linear regression or least-squares analysis. We include a point-by-point weighting factor to the least-squares method and show that the complexity of the calculation is not significantly increased.

As an example, consider the case of a single KB mirror, with two bending couples, one at each end. For simplicity, we will concentrate our attention on these two degrees of freedom, but the method is extendable to an arbitrary number of independent degrees. The shape is measured as a trace with N points, labeled x_i, and the measured mirror heights are given by y_i. Let the ideal mirror shape be y_i^0. The two characteristic functions, defined as changes induced by small actuations of the benders, are $f_1(x_i)$ and $f_2(x_i)$. We introduce a constant value, a_0, to accommodate any residual offsets in the measurements, which are not physically important for focus optimization. (Note that a_0 is associated with a constant characteristic function $f_0(x_i) = 1$.) The surface height error that we seek to optimize, h_i, is the difference between the measured and the ideal shapes, after the optimal bending has been applied. In other words, after bending, the remaining shape error described by h_i provides the highest possible Strehl ratio. Combining these, we can write the shape measured at each point as

$$y_i = y_i^0 + a_0 + a_1 f_1(x_i) + a_2 f_2(x_i) + h_i. \quad (10)$$

B. Applying the least-squares method

An optimized solution comes from the minimization of an error function, S, equal to the sum of the squares of the height errors, h_i, weighted point-by-point by w_i. We can expand this as

$$S = \sum_i w_i h_i^2 = \sum_i w_i \left[y_i - y_i^0 - a_0 - a_1 f_1(x_i) - a_2 f_2(x_i)\right]^2. \quad (11)$$

This discrete summation is analogous to minimizing $\int A_C(x)[h(x)]^2 dx$, as discussed above.

It can be shown that a solution with the least-squares method[27] is mathematically equivalent to that given by linear regression. An example of the general regression approach is described in Ref. 28, with and without weighting, and is described with characteristic functions in Ref. 29.

In both methods, the optimal solution is found with respect to each degree of freedom a_j. Setting

$$\frac{\partial S}{\partial a_j} = 0 \tag{12}$$

for each j results in a system of linear equations. In the least-squares method, the matrix expression may be written directly in the form

$$\begin{pmatrix} \Sigma w_i & \Sigma w_i f_1(x_i) & \Sigma w_i f_2(x_i) \\ \Sigma w_i f_1(x_i) & \Sigma w_i f_1(x_i)^2 & \Sigma w_i f_1(x_i)\, f_2(x_i) \\ \Sigma w_i f_2(x_i) & \Sigma w_i f_1(x_i)\, f_2(x_i) & \Sigma w_i f_2(x_i)^2 \end{pmatrix} \begin{pmatrix} a_0 \\ a_1 \\ a_2 \end{pmatrix} = \begin{pmatrix} \Sigma w_i (y_i - y_i^0) \\ \Sigma w_i f_1(x_i) \left(y_i - y_i^0\right) \\ \Sigma w_i f_2(x_i) \left(y_i - y_i^0\right) \end{pmatrix}. \tag{13}$$

Solution for the unknown coefficients comes from inverting the *curvature matrix* and solving as with any linear system of equations. Note that in the un-weighted solution, w_i is set to 1, and Eq. (13) is simplified.

The formulation of Eq. (13) assumes that each position's height measurement has the same uncertainty. This is a reasonable assumption for both profilometry and interferometric wavefront measurement (at-wavelength or otherwise). If the measurement uncertainty varies from point to point, as σ_i, that information can be included in the weightings with a $1/\sigma_i$ multiplier,[30] attributing lower weight where uncertainty is higher.

There are a few issues that warrant caution in the application of either linear regression or the least-squares method. Interdependence among the actuations, and other sources of non-linearity in the system response, can be overcome with additional iterations and by taking smaller steps toward optimization. Motion hysteresis, mechanical tolerances in the actuators, and noise in the position encoders can set a lower limit on the optimization that can be achieved deterministically. Also, redundancy among the degrees of freedom causes degeneracy in the characteristic functions, which can cause the solution to become ill-conditioned. When that happens, the calculation may recommend inappropriately large actuations from multiple degrees of freedom.

VI. MATHEMATICAL DEMONSTRATIONS OF MIRROR OPTIMIZATION WITH DIFFERENT WEIGHTINGS

In this section, we demonstrate simulated 1D beam focusing based on mirror shape optimizations performed using only the available characteristic shape changes. Two demonstrations show the potential significance of weighting in the optimization of the Strehl ratio.

Consider a hypothetical KB mirror with two bending couples, one on each end. For small actuations, the change in the surface height is shown in Fig. 6. These are the characteristic functions, and they approximate those found experimentally, by the authors, on a single KB mirror under test.[1,2]

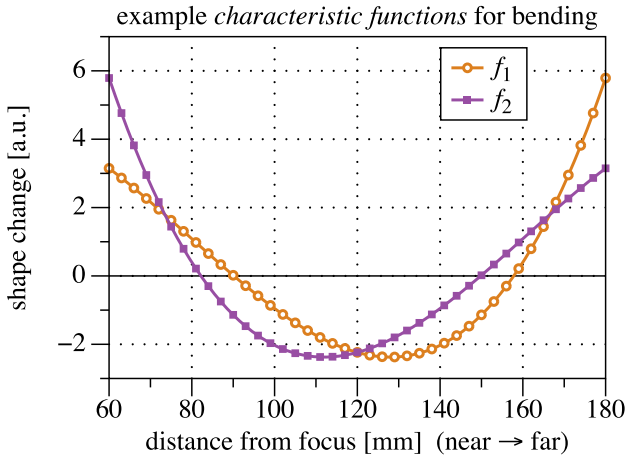

FIG. 6. Characteristic bending functions from a single, hypothetical KB mirror. These are the degrees of freedom used in the simulated mirror optimization. The near side (closer to focus) and far side of the mirror are indicated.

For this focusing optimization example, we study three different weightings based on the beam's intensity distribution across the mirror surface and on the reciprocal of the distance (from points on the mirror to the ideal focus). In other words, $I(x)/s(x)$. See Fig. 7. (Additional physical parameters could be included in the same manner.) Case A begins with uniform illumination and is weighted by a factor equal to 1/distance. The other two, B and C, have centered Gaussian weightings for the beam intensity to which the reciprocal distance weighting is applied. Defined on normalized coordinates [−1, 1], the power weightings follow $\exp[-(1.25x)^2]$ and $\exp[-(2.5x)^2]$, for B and C, respectively. For all three, the power weighting is normalized before the distance weighting is applied, so mathematically, the same integrated power level falls on each mirror, across its surface.

The optimization uses the two available degrees of freedom (i.e., by adding or subtracting independent amplitudes

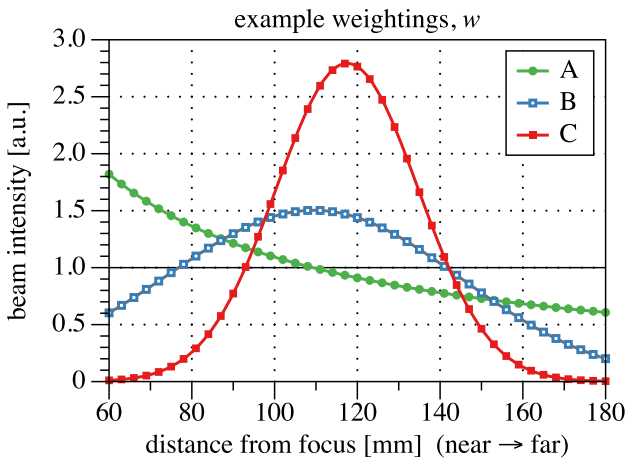

FIG. 7. Three sample weighting functions for the simulated optimization. Each includes the reciprocal distance weighting for the mirror described in Section III. The other factors are (A) uniform, (B) and (C) centered Gaussian. The near side (closer to focus) and far side of the mirror are indicated.

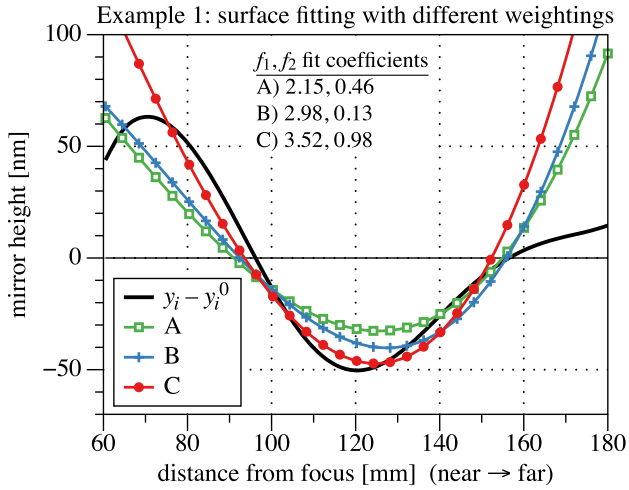

FIG. 8. Example 1. Three weighted fittings to the height error function (black line).

of the two characteristic functions) to balance the aberrations based on these three different weightings. Then the focal plane image (focal spot) is calculated in each case using illumination (C), the most narrow, concentrated-light case. In the calculation, the field is propagated from the mirror surface to the focal plane using a full wave-based treatment, similar to Eq. (2), but calculated for each point in the focal plane in the vicinity of the ideal focus.

We consider two different surface fitting examples. Figures 8 and 9, respectively, show the different weighted fittings to the original surface height errors (black lines). The fits labeled C appear different from the other two because the weighting is concentrated near the center. Consequently, for case C, fitting at the edges, where the light level is low, is less important. The best-fit coefficients of the characteristic functions are shown for each case within Figs. 8 and 9. The coefficients can be significantly different for the three optimizations, including having different amplitude *and sign*. Note that these calculations are performed on a simulation domain with 5001 points along the mirror surface, but for presentation, the plots in Figs. 8 and 9 show only 41 points.

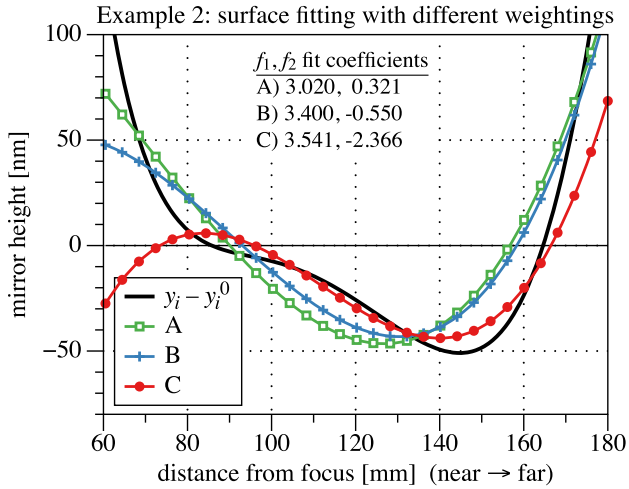

FIG. 9. Example 2. Three weighted fittings to the height error function (black line).

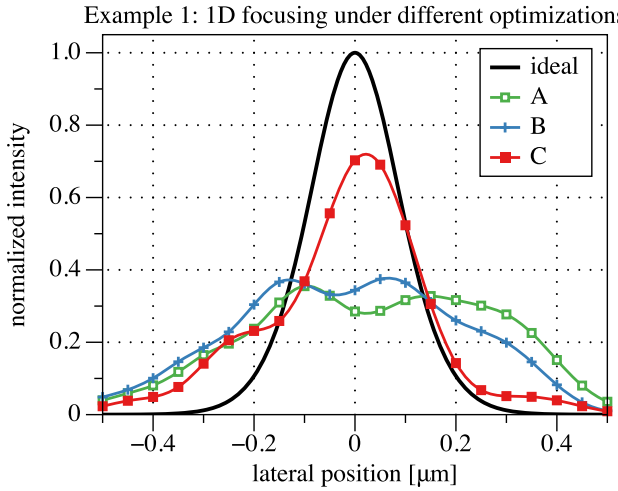

FIG. 10. Calculated focal plane intensities for example 1 with three centered weightings. From the ideal case, and cases A, B, and C, respectively, the FWHM values are {209, 665, 606, and 239 nm}, and the Strehl ratios are {1, 0.355, 0.377, and 0.720}.

Based on these optimizations, the resulting focal plane intensities from the two examples are shown in Figs. 10 and 11, respectively. As expected, we find that the highest Strehl-ratio (central intensity) comes from optimization performed with the weighting that matches the beam power (and distance) used in the focal intensity calculations. The Strehl ratios are given in the figure captions. The focal plane intensity is calculated with 2-nm spacing, but for clarity, the plots points in Figs. 10 and 11 are spaced by 50-nm.

VII. DISCUSSION

High-brightness short-wavelength light sources will only achieve their full potential in nanoscience applications when the optical systems designed for focusing can be optimized reliably. Developing effective strategies for *ex situ* and *in situ* optical alignment, suitable for sub-100-nrad slope errors and

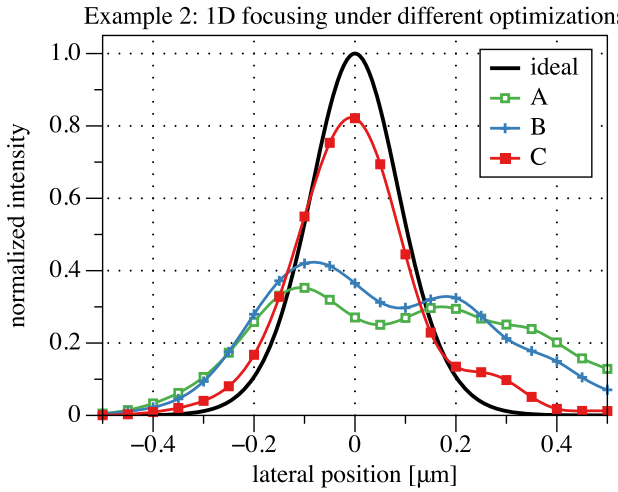

FIG. 11. Calculated focal plane intensities for example 1 with three centered weightings. From the ideal case, and cases A, B, and C, respectively, the FWHM values are {209, 674, 533, and 237 nm}, and the Strehl ratios are {1, 0.353, 0.423, and 0.823}.

sub-100-nm focusing, requires improvement over the current state of the art.

We have shown that accounting for the well-understood physical effects contributing to focusing can have a profound effect on focal intensity and light distribution in the focal plane. In addition to the varying distance from focus for points along the mirror's surface, the incident beam's power distribution and angles of incidence and the mirror's local reflectivity (including a contamination distribution, if known) can all be incorporated into the optimization algorithm. Many of these effects can be measured directly, for use in the optimization algorithm, by recording the light intensity distribution in a plane far from focus. Adding these effects does not increase the mathematical complexity of the solution using standard deterministic approaches such as least-squares or linear regression. This work builds on prior work from Mahajan and others who described ways to accommodate pupil shapes and vignetting into Strehl ratio calculations.

When at-wavelength interferometry is performed on a beamline, many of the variables related to the physical transmission of light through an optical system can be extracted directly from the data. For example, by projecting the illuminating beam through the system without interference and measuring the intensity profile in a plane far from focus, the combined physical mechanisms that affect the transmitted beam's intensity distribution will be revealed. Those effects can be incorporated in the optimization algorithm without additional calculations or reliance on imperfect knowledge of the optical system's spatially varying properties.

It is challenging to generalize the effectiveness of this weighted optimization because every optical system and beamline are unique. Outcomes will strongly depend on the illuminating beam's power distribution and the profile of the mirror height aberrations not reducible through compensation. The method presented here should be generally effective for a variety optical systems and is not limited to glancing-incidence in any way.

Separate considerations, beyond the scope of this method, should be made for solving a different important problem in modern X-ray optics: the creation of uniform sample illumination. The method here pertains well to focusing and the optimization of the peak intensity on axis. Creating uniform beam profiles by mirror actuation is a much more challenging task for which these methods may not apply.

ACKNOWLEDGMENTS

This work was performed by scientists from the Center for X-Ray Optics and the Advanced Light Source at Lawrence Berkeley National Laboratory. The Advanced Light Source is supported by the Director, Office of Science, Office of Basic Energy Sciences, of the U.S. Department of Energy under Contract No. DE-AC02-05CH11231. The authors are indebted to Wayne McKinney, Sheng Yuan, Daniel Merthe, Iacopo Mochi, and James Macdougall among others who have contributed in this area.

[1]S. Yuan, K. A. Goldberg, V. V. Yashchuk, R. Celestre, I. Mochi, J. Macdougall, G. Y. Morrison, W. R. McKinney, M. Church, and T. Warwick, Proc. SPIE **7801**, 78010D (2010).
[2]D. J. Merthe, V. V. Yashchuk, K. A. Goldberg, M. Kunz, N. Tamura, W. R. McKinney, N. A. Artemiev, R. S. Celestre, G. Y. Morrison, E. Anderson, B. V. Smith, E. E. Domning, S. B. Rekawa, and H. A. Padmore, Proc. SPIE **8501**, 850108 (2012).
[3]W. R. McKinney, V. V. Yashchuk, K. Goldberg, D. J. Merthe, and N. A. Artemiev, Proc. SPIE **8501**, 850109 (2012).
[4]V. V. Yashchuk, D. J. Merthe, K. A. Goldberg, N. A. Artemiev, R. Celestre, E. E. Domning, M. Kunz, W. R. McKinney, G. Y. Morrison, B. V. Smith, and N. Tamura, J. Phys.: Conf. Ser. **425**, 152003 (2013).
[5]K. Strehl, Z. Instrumentenkd. **22**, 213 (1902), available at http://hdl.handle.net/2027/hvd.hx69uc?urlappend=%3Bseq=253.
[6]V. N. Mahajan, *Optical Imaging and Aberrations, Part II: Wave Diffraction Optics*, 2nd printing ed. (SPIE Press, 2004).
[7]M. Born and E. Wolf, *Principles of Optics*, 5th ed. (Pergamon, New York, 1975), p. 482.
[8]V. N. Mahajan, J. Opt. Soc. Am. **72**, 1258 (1982).
[9]D. D. Lowenthal, Appl. Opt. **13**, 2126 (1974).
[10]R. Barakat, J. Opt. Soc. Am. **70**, 739 (1980).
[11]V. N. Mahajan, J. Opt. Soc. Am. A **22**, 1824 (2005).
[12]R. Herloski, J. Opt. Soc. Am. A **2**, 1027 (1985).
[13]R. Barakat and A. Houston, J. Opt. Soc. Am. **55**, 538 (1965).
[14]M. Vannoni, F. Yang, F. Siewert, and H. Sinn H, Proc. SPIE **9208**, 92080I (2014).
[15]P. Kirkpatrick and A. V. Baez, J. Opt. Soc. Am. **38**, 766 (1948).
[16]L. Raimondi and D. Spiga, Proc. SPIE **7732**, 77322Q (2010).
[17]L. Raimondi and D. Spiga, Astron. Astrophys. **2014**, 24907.
[18]E. L. Church and P. Z. Takacs, Appl. Opt. **32**, 3344 (1993).
[19]J. Goodman, *Introduction to Fourier Optics*, 3rd ed. (Roberts and Company Publishers, 2004).
[20]O. Chubar, L. Berman, Y. S. Chu, A. Fluerasu, S. Hulbert, M. Idir, K. Kaznatcheev, D. Shapiro, Q. Shen, and J. Balster, Proc. SPIE **8141**, 814107 (2011).
[21]M. Bowler, J. Bahrdt, and O. Chubar, "Wavefront propagation," in *Modern Developments in X-Ray and Neutron Optics* (Springer, Berlin, 2008), Vol. 137.
[22]V. V. Yashchuk, L. V. Samoylova, and I. V. Kozhevnikov, Opt. Eng. **54**, 025108 (2015).
[23]S. Szapiel, Opt. Lett. **2**, 124 (1978).
[24]S. Szapiel, J. Opt. Soc. Am. **72**, 947 (1982).
[25]V. N. Mahajan, J. Opt. Soc. Am. **73**, 860 (1983).
[26]O. Hignette, A. K. Freund, and E. Chinchio, Proc. SPIE **3152**, 188–199 (1997).
[27]P. R. Bevington and D. K. Robinson, *Data reduction and Error Analysis for the Physical Sciences*, 2nd ed. (McGraw Hill, 1992), Chap. 7.
[28]V. V. Yashchuk, Proc. SPIE **6317**, 63170A (2006).
[29]W. R. Mckinney, J. L. Kirschman, A. A. MacDowell, T. Warwick, and V. V. Yashchuk, Opt. Eng. **48**, 083601 (2009).
[30]P. R. Bevington and D. K. Robinson, *Data reduction and Error Analysis for the Physical Sciences*, 2nd ed. (McGraw Hill, 1992), Chap. 4.